Ejecta from periodical grooves in tin foils under laser-driven shock loading

G. Prudhomme, J.-E. Franzkowiak, T. de Resseguier, E. Brambrink, C. Roland, Didier Loison, E. Lescoute, A. Sollier

Ejecta from Periodical Grooves in Tin Foils under Laser-Driven Shock Loading

G. Prudhomme[1,a)], J-E. Franzkowiak[1], T. de Rességuier[4], E. Brambrink[2,3], C. Roland[1,4], D. Loison[5], E. Lescoute[1] and A. Sollier[1]

[1] *CEA, DAM, DIF, F-91297 ARPAJON*

[2] *LULI - CNRS, Ecole Polytechnique, CEA, Université Paris-Saclay, F-91128 PALAISEAU cedex*

[3] *Sorbonne Universités, UPMC Univ. Paris 06, CNRS, Laboratoire d'Utilisation des Lasers Intenses (LULI), place Jussieu, F-75252 PARIS cedex 05*

[4] *Institut Pprime, CNRS, ENSMA, Univ. Poitiers, 1 av. Clément Ader, F-86960 FUTUROSCOPE*

[5] *IPR, CNRS, Univ. Rennes 1, F-35042 RENNES*

[a)]Corresponding author: gabriel.prudhomme@cea.fr

Abstract. Laser-driven shock loading is a versatile, low destructive method to study material dynamic behaviors with an efficient repetitive rate. In these experiments, compared with the more conventional high-explosive or impact-based techniques, all the scales are reduced (few ns shock duration, a few mm planar loaded area) while the shock pressure may reach several tens of GPa. This configuration makes possible the use of many diagnostics with limited exposition to generated fragments.

We present recent experiments of material ejection under laser-driven shock loading. The target is a thin plate of Tin with periodical grooves of few tens of μm in its rear surface, in order to induce solid or liquid micro-jetting. These jets turn into a cloud of μm-sized particles. Depending on surface roughness, the velocity and the density of the cloud vary. The density of the cloud is estimated thanks to a new high-resolution X-ray imaging with a laser-driven source; while optical shadowgraphy observes the displacement of the fastest particles. Thus, μm-structures in the particles cloud and in the target can be revealed.

INTRODUCTION

KiloJoule-laser driven shocks are powerful tools for studying micro-jetting [1, 2]. Because they are not very destructive, all the diagnostics can be very close to the ejecta area (down to a few mm), they allow several experiments in the same day (up to 10), the shock pressure is adjustable (the laser fluence or the spot diameter), all the delays are adjustable (unlike the guns). However, the shockwave flatness is not perfect: most of the time, the laser spot diameter is spread out to have a nearly plane shockwave in the center of the spot (about a few mm).

(Micro)jetting has been studied for many years [3]. The areal mass, the velocity and the particle diameters are the major issues to qualify ejecta. In most of the experiments, ejecta is considered as a 1D phenomena, measured and associated with global parameters. A typical instance is the areal mass, which is measured by Asay foils, piezoelec-tric probes or X-rays. More recently, the understanding of microjetting physics required experiments in which jets (spikes) and bubbles are well resolved. In this case, perturbation lengths are usually greater than 200 μm, with depths greater than 50 μm. This paper describes recent experiments achieved in the LULI2000 facility. Thanks to a ultrashort (picosecond) laser-generated X-ray source [4], it is possible to resolve the microjets coming from micrometric shapes, the sizes of them are comparable to conventional machining roughness (down to 8 μm perturbation amplitude).

Like High Explosive (HE) generators, the shockwave is unsteady and leads to microspall. The jets are followed by a microspall cloud, the density of which seems to be perturbed by the jet growth.

Experimental setup

The setup is described in Figure 1. A ns-pulsed laser is aimed at the front surface of the target. The wavelength of this laser is 1064 nm, the pulse duration is 4.0 ns and the spot diameter is 1.5 mm for all the experiments presented in this paper. The experimental velocity of the free polished surface is 2,700 m/s, the induced shock-breakout pressure is estimated at 45 GPa [5]. Thanks to this high pressure (above 32 GPa), shocked Tin is in a liquid state after release [6]. The absorption of X-rays is related to the density of the ejecta, and recorded on an image plate. A dual multi-frame shadowgraphy axis is used to observe the velocity of the fastest particles and the flatness of the shockwave in the X-ray direction. Radiographic and shadowgraphy axes are perpendicular each other. Note that the same setup was used to investigate microjetting from single grooves of triangular shape in various metals, as reported in another contribution [7].

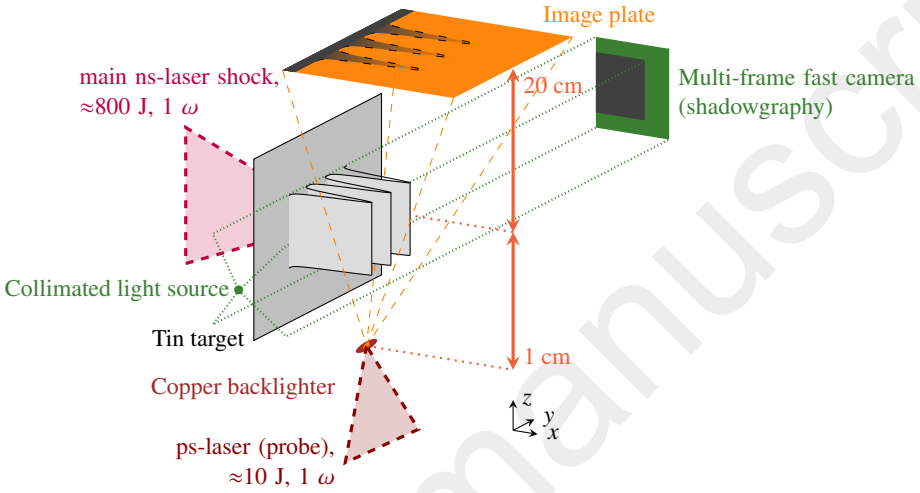

FIGURE 1. Experimental setup: dual shadowgraphy and X-ray imaging.

Target characterization

Targets are made of 230 μm-thick pure Tin (> 99.7 %) foils. The rear surfaces have been optically polished and then machined using laser ablation. The roughness is a juxtaposition of sinus-like shapes along shadowgraphy axis (y). Their perturbation amplitudes, peak-valleys and wavelengths are respectively written down η, $h = 2\eta$ (from 8 to 32 μm), and λ (from 60 to 180 μm). These values are measured using confocal microscopy. The machined area is a rectangle, almost a square, the side along radiographic axis (z) is 1 mm length and the other side is close as possible to 1 mm in order to get an entire number of shapes. The shape factor $k\eta = 2\pi\frac{\eta}{\lambda} = \pi\frac{h}{\lambda}$ of the roughness is defined as the ratio between the amplitude and the perturbation wavelength [8].

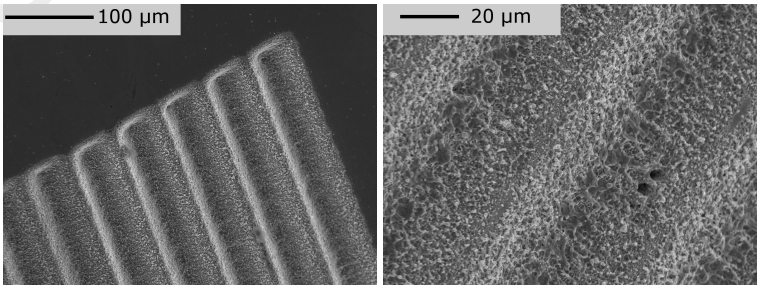

FIGURE 2. Examples of Scanning Electron Microscope (SEM) images from one target.

X-ray imaging

The X-ray laser-driven source is made of a Copper microwire (about 20 μm), heated by a 1 ω, 1.5 ps, 10 J laser. Irradiation is strong enough to produce Kα photons [4], at 8.022 keV. A very high magnification (21x) is obtained by the proximity of the Copper backlighter to the ejecta.

The magnification (21x) and the resolution (20 μm FWHM) of the X-ray imaging are evaluated by a grid located in the ejecta plane. The Line Spread Function (LSF) is computed from the image of this grid (Figure 3). Due to the very short duration of the pulse, the motion blur is negligible (about 15 nm for an object moving at 10 km/s).

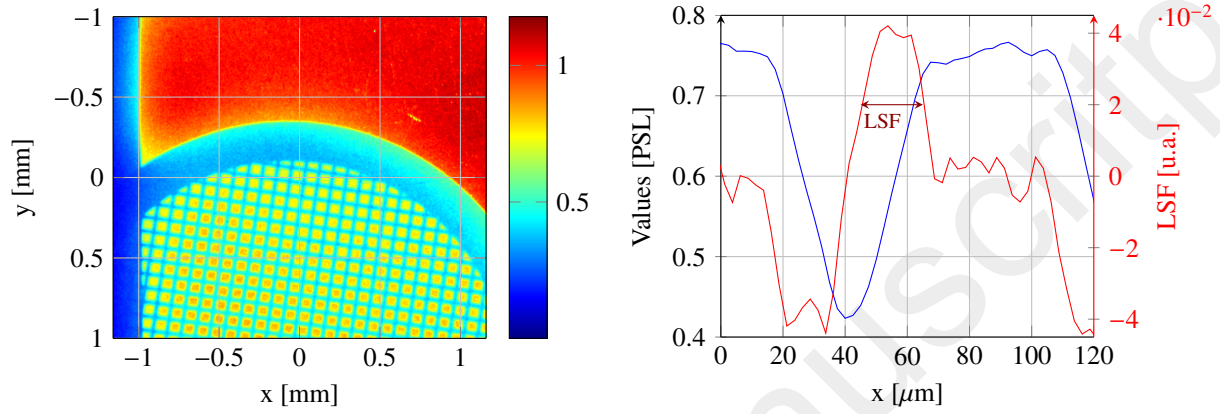

FIGURE 3. Estimation of the X-ray imaging resolution. On the left, the image of a 300 lp/inch grid. On the right, the image profile of one edge and the associated LSF.

EXPERIMENTAL RESULTS

Velocity of the fastest particles from the shadowgraphy

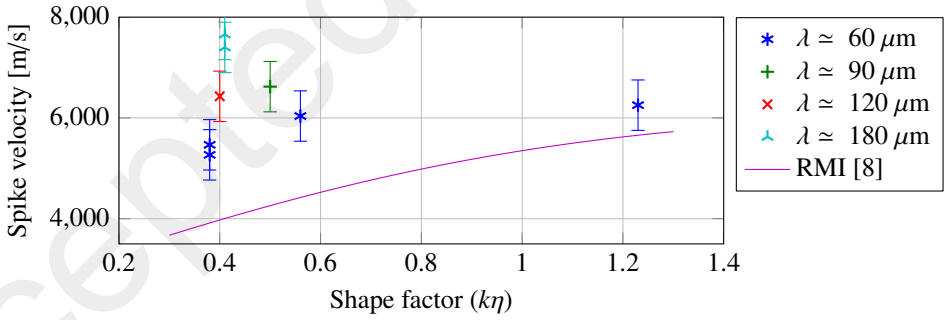

FIGURE 4. Velocity of the fastest particles, as a function of the shape factor of the roughness ($k\eta$), and different perturbation wavelengths (λ). The error bars (±500 m/s) are derived from an estimated accuracy of the cloud-front visual identification.

The velocity of the cloud front, composed of the fastest particles, has been measured using a multi-frame shadowgraphy (Figure 4, see [2] for an example). Velocity is close to be constant, calculated from first images recorded at 70 and 110 ns after the laser shock. Because all the perturbation amplitudes are weaker than the perturbation wavelengths ($k\eta \lesssim 1$), the Richtmyer-Meshkov Instabilities (RMI) framework is used to discuss our results. In Figure 4, we can observe that:

- For the smallest defects, the spike velocity follows the RMI trend, despite the fact that velocities are much faster than RMI prediction.

- The spike velocity increases with the perturbation wavelength (and a very similar shape factor $k\eta$). This result, which is not predicted by RMI, may be a consequence of the large decrease of the shockwave pressure with the thickness of the target (the initial shock at the front face is only steady for a few ns). As a consequence, the shockwave velocity may be underestimated in the RMI used here for large scales (λ).

Examples of X-ray Images

Two examples of X-ray images are presented below, the ratio of the sizes of the roughness is 3, between both images (Figure 5). Jets are resolved (different scales), and complexity of their growth is revealed:

- The bubbles are slower than the free surface [8].
- Jet expansion clearly affects the microspall.
- Jets fragment into particles. The typical time required to make the cloud homogeneous appears to be a function of the typical sizes of the roughness.

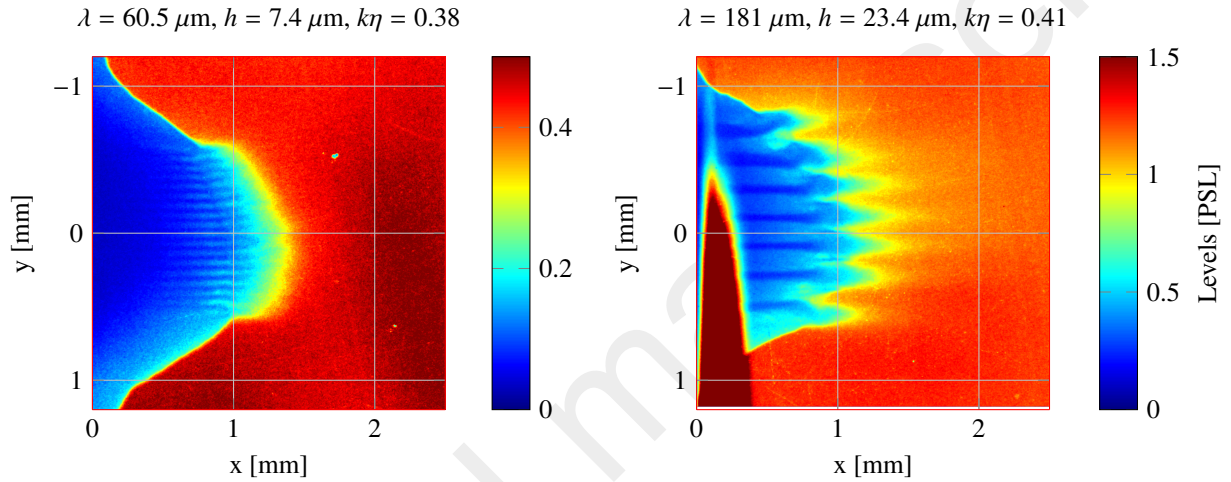

FIGURE 5. Two examples of X-ray images. Both images are recorded 400 ns after the laser shock, both targets share the same shape factor (about $k\eta \simeq 0.40$); however the dimension of the initial roughness is almost tripled on the second image. The shadow on the bottom left of the image on the right hand side is a X-ray leak coming from plasma produced by the ns-laser. In this case, either the target is not well pinned to its holder or the target is torn by the shock. More investigation is required to understand this phenomenon.

Ejecta mass

The absorption of the X-ray is related to the product of the Tin density and cloud depth. Supposing that this depth is equal to the side length of the grooved zone (1 mm), this density may be estimated at each pixel of the cloud. Next, the mean density across the y-axis is computed and used to get access to the cumulated ejected mass M_e. (comparable to what can be measured by a *Asay* foil [9] or by a piezoelectric probe). The ejected total mass is equal to the cumulated mass at the location of the free surface. This location is determined with another experiment using a polished area on the rear surface.

Because the Defect Mass per unit Area (DMA) is proportional to $h \propto \eta$, the ejected mass should be related to a variation of η. Two comparisons can be underlined:

- Similar shape factor but two different wavelengths (cyan and yellow curves). Cumulated areal mass at the free surface is about 11 mg.cm^{-2} for both curves. These curves do not grow at the same rate. Indeed, particle maximum velocities are higher for large wavelengths (as previously shown by shadowgraphy, Figure 4). Moreover, several models, as Dimonte et al.'s fit [10, eq. 5.2] or the analytic expression by Cherne et al. [11, eq. 6] lead to an increase of the areal mass with the perturbation amplitude $\propto h$ and the wavelength λ; thus

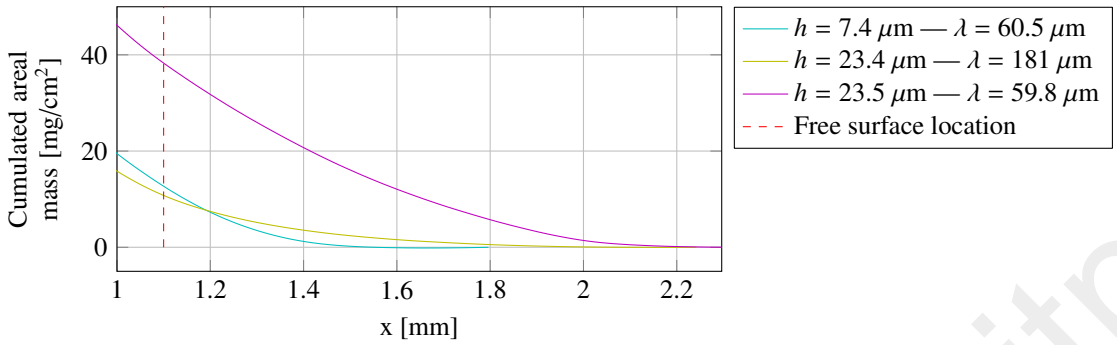

FIGURE 6. Cumulated ejecta mass for 3 shots. The radiography is captured 400 ns after the laser shock.

the value of the yellow curve at the free surface should be expected to be much larger. In this case, the jets are resolved (Figure 5), the density of tin could be higher in spikes and our current fit may be inaccurate for such densities.

- Different shape factor and the same wavelength (cyan and purple curve). Here, the shape factor $k\eta$ is tripled, and the areal mass at the free surface is multiplied by 3.5.

These results partially follow the "defect volume" model [12], which relates the ejected mass and the peak-valley h.

CONCLUSIONS

Laser-shock generators can produce liquid μm-scale microjetting from periodical patterns. Using the ps-laser generated X-ray source, high-resolution (≈20 μm FWHM) imaging measures the density of the cloud. This density, and the derived areal mass, can be compared to the perturbation amplitude and wavelength, or the ratio of both called shape factor.

This experimental design could be used to explore ejecta physics, in particular for parametric studies. Moreover, laser-produced ejecta could be well characterized due to the large number of simultaneous diagnostics (Photonic Doppler Velocimetry (PDV), X-ray, shadowgraphy, . . .). One can cross-correlate measurements in the same realization of an experiment. At least, due to the localization of the laser shock, which reduces the need to confine the blast and fragments, and the high rate of experiments (up to 10 each day), new diagnostics could be easily set up, tested and qualified.

ACKNOWLEDGMENT

The access to the *Laboratoire pour l'Utilisation des Lasers Intenses* (LULI) facility was allocated by the Institut Laser Plasma (ILP, FR #2707). We thank all the *NANO2000* staff for their technical support.

REFERENCES

[1] T. de Rességuier et al. In: *Journal of Applied Physics* 115.4 (2014). ISSN: 0021-8979. DOI: 10.1063/1.4863719.
[2] T. de Rességuier et al. In: *Journal of Applied Physics* 119.18 (2016), p. 185108. DOI: 10.1063/1.4949483.
[3] W. T. Buttler, R. J. R. Williams, and F. M. Najjar. In: *Journal of Dynamic Behavior of Materials* (May 22, 2017). ISSN: 2199-7454. DOI: 10.1007/s40870-017-0120-8.
[4] H.-S. Park et al. In: *Physics of Plasmas* 15.7 (2008), p. 072705. DOI: 10.1063/1.2957918.
[5] C Mabire and P.-L. Hereil. In: *Journal de Physique IV* 10.P9 (2000). 6th International Conference on Mechanical and Physical Behaviour of Materials Under Dynamic Loading, Krakow, Poland, SEP 25-29, 2000, 749–754. ISSN: 1155-4339. DOI: 10.1051/jp4:20009124.

[6] M. B. Zellner et al. In: *Journal of Applied Physics* 103.12 (2008), p. 7. ISSN: 0021-8979. DOI: 12350210.1063/1.2939253.
[7] T. de Rességuier et al. In: *Submitted to this conference*. 2017.
[8] W. T. Buttler et al. In: *Journal of Fluid Mechanics* 703 (July 25, 2012), pp. 60–84. ISSN: 0022-1120. DOI: 10.1017/jfm.2012.190.
[9] J. R. Asay, L. P. Mix, and F. C. Perry. In: *Applied Physics Letters* 29.5 (1976), pp. 284–287. ISSN: 0003-6951. DOI: 10.1063/1.89066.
[10] G. Dimonte et al. In: *Journal of Applied Physics* 113.2 (2013), p. 19. ISSN: 0021-8979. DOI: 10.1063/1.4773575.
[11] F. J. Cherne et al. In: *Journal of Applied Physics* 118.18 (2015), p. 185901. DOI: 10.1063/1.4934645. eprint: https://doi.org/10.1063/1.4934645.
[12] J. R. Asay and L. D. Bertholf. Tech. rep. SAND78-1256. Sandia Laboratories, Oct. 1978.